Textile & Leather Review

ISSN 2623-6281| www.tlr-journal.com | 10.31881/TLR

Optimization of Color Stability of Chinese Garden-Style Printed Fabrics: Dyeing and Finishing Process Based on GraphSAGE-BiLSTM

Lin Zhou

How to cite: Zhou L. Optimization of Color Stability of Chinese Garden-Style Printed Fabrics: Dyeing and Finishing Process Based on GraphSAGE-BiLSTM. Textile & Leather Review. 2026; 9:326-350. https://doi.org/10.31881/TLR.2026.326

How to link: https://doi.org/10.31881/TLR.2026.326

Published: 28 February 2026

Optimization of Color Stability of Chinese Garden-Style Printed Fabrics: Dyeing and Finishing Process Based on GraphSAGE-BiLSTM

Lin Zhou

School of Design, Jiangnan University, Wuxi 214122, Jiangsu, China

LINZHOU7787@163.com

Article

https://doi.org/10.31881/TLR.2026.326

Received 30 July 2025; Accepted 22 September 2025; Published 28 February 2026

ABSTRACT

This paper addresses the technical challenges of dye migration (ink bleeding), attenuation of color fastness in high-saturation color blocks, and pattern blurring—unintended negative consequences arising from the pursuit of the artistic "ink-wash diffusion effect" in the dyeing and finishing of Chinese garden-style printed fabrics. An intelligent optimization method based on GraphSAGE-BiLSTM is proposed. By constructing a dyeing and finishing knowledge graph, the compatibility constraints of reactive dyes and color fixatives within the dye-auxiliary-fiber ternary interaction network, as well as the influence of process parameters, are quantified. A dual-channel cross-modal learning model is designed, utilizing GraphSAGE (Graph Sample and Aggregation) to learn the characteristics of the dye auxiliary network. BiLSTM (Bidirectional Long Short-Term Memory) decodes the dynamic effects of the evaporation temperature curve and washing sequence and optimizes feature weights via an attention mechanism. Finally, the Pareto optimal process solution is generated by combining the NSGA-II (Non-dominated Sorting Genetic Algorithm II) multi-objective optimization algorithm. Experimental results show that this method improves color fastness from level 3.0 (control group) to level 4.5 (on a 1–5 scale) and reduces color difference from 1.80 to 1.20 (a decrease of 33.3%). Additionally, it reduces the amount of auxiliary agents in group B with medium-intensity process parameters by 10% and the energy consumption of washing by 14.5%. This study enables collaborative modeling of structured rules and temporal dynamics in dyeing and finishing processes and provides an industrializable pathway for improving color stability in cultural and creative textiles.

KEYWORDS

Chinese garden-style textiles, color stability optimization, dyeing and finishing process, GraphSAGE-BiLSTM model, knowledge graph

INTRODUCTION

As a representative of cultural and creative textiles, the artistic value of Chinese garden-style printed fabrics

depends on the precise presentation of the composition concept of “white as black” and the color rule of “coloring according to the type.” The core lies in the gradient of ink color, color fastness of high-saturation color blocks, and the clarity of fine pattern edges [1,2]. However, the complex dyeing and finishing process designed to achieve the ink-wash effect often leads to severe damage to color stability: the ink-wash gradient area becomes blurred due to the migration of dye molecules [3,4]; high-saturation color blocks undergo co-hydrolysis during the evaporation stage, resulting in attenuation of color fastness [5,6]; and the outlines of fine pavilions are blurred due to residual floating color after washing [7,8]. These issues often lead to the degradation of high-end fabrics because of color distortion, highlighting the core contradiction between traditional aesthetic expression and the stability of industrial production. Although existing studies adjust process parameters through orthogonal experiments, it is difficult to quantify the nonlinear influence of dye-auxiliary compatibility rules [9,10]. When LSTM predicts static parameters, it ignores the coupling between the cumulative effect of steaming temperature time series and the dynamic change of washing intensity [11,12]; there is also a lack of systematic modeling of structural constraints, such as anionic/cationic electrical conflicts and reactive dye hydrolysis kinetics, making optimization efficiency difficult to meet industrial needs [13,14].

Currently, research on color fastness optimization of printed fabrics is trending toward multiple technical paths. Uğur [15] proposed a wet processing technology for cotton fabrics based on LbL (Layer-by-Layer), integrating dyeing and functional finishing through cationic modification, which effectively reduces water and chemical consumption. However, multilayer deposition easily damages the silk texture, and industrial energy consumption and cost verification remain insufficient. Liang et al. [16] used bio-based gardenia blue ink to modify the surface of silk fabrics with polysaccharide derivatives, achieving high-quality printing performance. The printed silk exhibited acceptable friction resistance and soap washing color fastness, but the solution for improving wet friction fastness still needs optimization. In the field of plant-derived natural dyes, Rahayuningsih et al. [17] optimized the extract dyeing process and achieved optimal dyeing effect and performance standards comparable to synthetic dyes by adjusting various parameters. Repon et al. [18] pointed out that natural dyes have become an important direction for sustainable textile processing due to their biodegradability and UV resistance, but their lack of color fastness and poor chromatographic reproducibility remain bottlenecks for industrialization. Ömeroğulları’s [19] simplified pretreatment process reduced water and electricity consumption while maintaining color fastness, but the effect on dark colors and long-term ecological impact requires further verification. Although these studies have achieved certain

results, they still face three major challenges: quantifying compatibility rules, controlling dynamic process timing, and balancing cultural adaptability with industrial cost constraints. These factors make it difficult to collaboratively solve the unique challenges of Chinese garden-style fabrics.

Intelligent optimization of dyeing and finishing processes is shifting from single-point breakthroughs to system integration, from experience-driven to data- and knowledge-driven approaches. Deep learning and graph neural networks are increasingly penetrating core links. Ingle et al. [20] reviewed the application of ANN (Artificial Neural Network), CNN (Convolutional Neural Network), and GAT-Graph Attention Network throughout the dyeing and finishing process, promoting parameter optimization and automation but failing to address dynamic coupling modeling of multiple processes. Liang et al. [21] utilized spectral reconstruction and BP (Back Propagation) neural networks to achieve automatic color fastness rating, improving efficiency and objectivity, but lacking adaptability to complex textures. Şahin et al. [22] constructed a multi-parameter ANN model to improve color prediction accuracy, and Chen et al. [23] proposed a Transformer multi-output model integrating physical knowledge to enhance interpretability. However, research faces limitations such as high industrial deployment costs and substantial prediction deviations for anthraquinone dyes. These studies reveal bottlenecks in weak cross-process coupling modeling and insufficient dynamic feature extraction capabilities, and a graph neural network joint time series modeling mechanism suitable for the entire dyeing and finishing process has yet to be established.

This paper constructs a knowledge graph in the field of dyeing and finishing, focusing on the ternary interaction network. Four types of entity nodes are defined: reactive dyes, color fixing auxiliaries, fiber substrates, and equipment parameters. Three types of edge relationships are also defined: chemical compatibility constraints, process impact weights, and environmental compliance rules. Compatibility constraints are quantified through Hirshfeld surface analysis and characterized multidimensionally by combining indicators such as ionic electrical matching. Based on the graph structure, the GraphSAGE-BiLSTM dual-channel architecture is designed: the GraphSAGE (Graph Sample and Aggregation) layer learns the compatibility characteristics of the dye node neighborhood and embeds the representation, while the BiLSTM layer decodes the evaporation temperature curve and the water washing flow time series dynamics. Dual-channel features are fused with weights dynamically assigned by a multi-head attention mechanism. Innovatively, a knowledge distillation mechanism is introduced, using the graph rules as teacher signals to constrain model learning. Finally, the NSGA-II algorithm is used to solve the Pareto optimal process solution, with wash fastness, color difference, and color penetration rate set as hard constraints, and process cost and

COD (Chemical Oxygen Demand) emissions as soft boundaries. This method enables collaborative decision-making based on chemical compatibility rules, time-series dynamics, and cultural-industrial needs for the first time, and proposes a quantifiable framework for the intelligent manufacturing of highly complex cultural textiles.

INTELLIGENT OPTIMIZATION FRAMEWORK FOR CHINESE GARDEN-STYLE PRINTING, DYEING, AND FINISHING PROCESSES

Overall Architecture Design for Color Stability Optimization

Figure 1 shows the color stability optimization framework for Chinese garden-style printed fabrics based on GraphSAGE-BiLSTM. The input layer receives printing pattern features, fabric substrate parameters, and process constraints, which are input into the dyeing and finishing knowledge graph module and the dynamic process time series acquisition module, respectively. The knowledge graph module uses heterogeneous graph structures (four types of nodes and three types of edges) to quantify the compatibility rules of dyes and auxiliaries. The time series acquisition module obtains real-time steaming temperature and washing flow data, forming a dynamic feature matrix after processing. The core GraphSAGE-BiLSTM fusion model extracts compatibility features via GraphSAGE, while the BiLSTM layer decodes the time-varying effects of temperature gradient and flow sequence, predicting indicators such as color difference and color penetration rate after multi-head attention fusion. The multi-objective optimization module, based on the NSGA-II algorithm, collaboratively optimizes color fastness, COD emissions, and additive dosage under constraints, outputs feasible solutions, and forms a closed-loop verification architecture. This architecture overcomes the bottleneck of insufficient quantification of compatibility rules and the separation of dynamic modeling in traditional methods, achieving collaborative decision-making for structured chemical rules and process sequence dynamics for the first time.

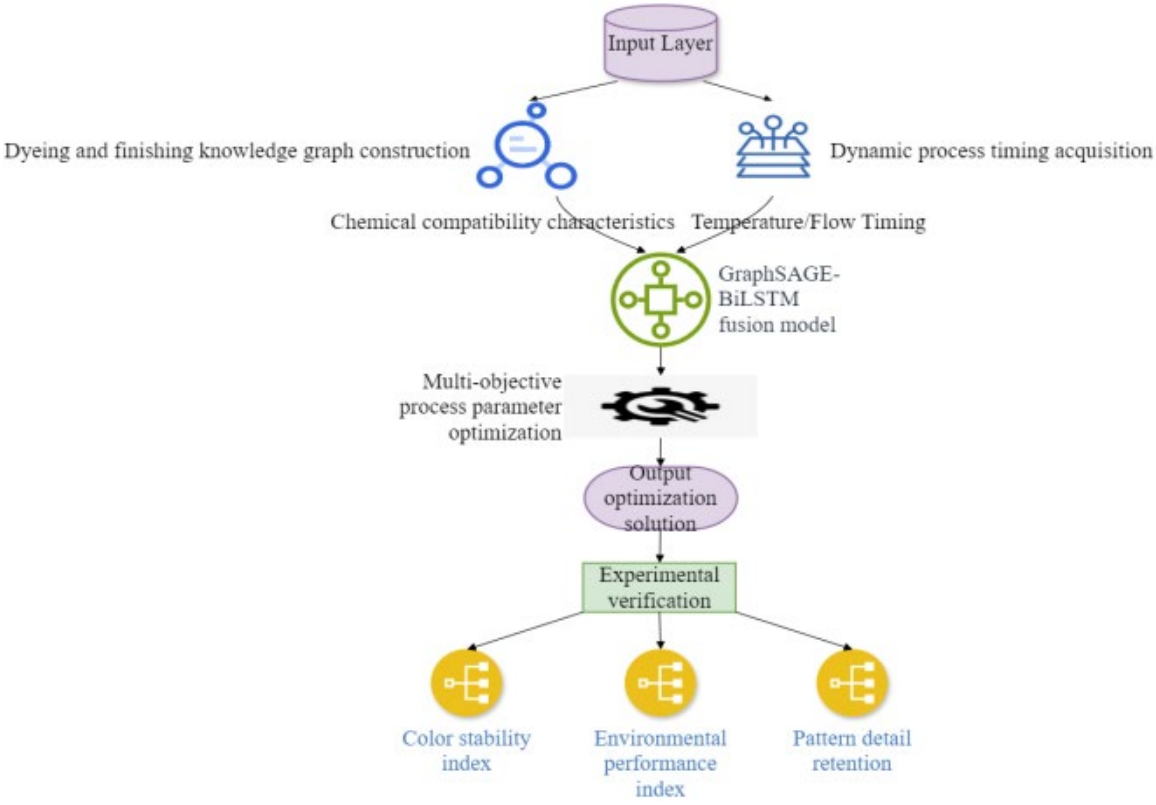

Figure 1. Overall framework of optimization design

Construction of Dyeing and Finishing Process Knowledge Graph

The construction of the dyeing and finishing process knowledge graph focuses on analyzing dye-auxiliary compatibility conflicts and process parameter coupling effects in Chinese garden-style printing [24]. Based on the ternary reaction system, a heterogeneous graph structure is constructed, including four types of entity nodes—reactive dyes, color fixation auxiliaries, fiber substrates, and equipment parameters—and three types of edge relationships: chemical compatibility constraints, process impact weights, and environmental compliance rules. Using Zeta potential measurement data, an ion electrical matching model is established to quantify compatibility constraints:

$$\varepsilon_{ij}=\frac{\left|\zeta_d-\zeta_f\right|}{\zeta_d+\zeta_f}\cdot\left(1-\frac{|Q_a-Q_c|}{\max(Q_a,Q_c)}\right) \quad (1)$$

In Formula 1, ε_{ij} is the electrical matching degree between dye i and auxiliary agent j, ζ_d and ζ_f

represent the Zeta potential of the dye and fiber, respectively and Q_a and Q_c are the charge densities of anionic/cationic auxiliary agents. The Zeta potentials are measured in mV at pH 7.0 and ionic strength 0.01 M using a Malvern Zetasizer Nano ZS. Reported values are the average of five repeated measurements, with a standard deviation of less than 5%.

The interaction strength is characterized in multiple dimensions by combining indicators such as electrostatic energy and matching score, drawing conceptual inspiration from the multifaceted analysis approach of Hirshfeld surface analysis.

According to the hydrolysis kinetics of reactive dyes, the Arrhenius correction equation is introduced to calculate the attenuation coefficient of the dye fixation rate:

$$k_{\mathrm{h}}=A\cdot e^{-\frac{E_a}{RT}}\cdot[OH^-]^{\alpha} \tag{2}$$

In Formula 2, k_{h} is the hydrolysis rate constant, A is the pre-exponential factor, E_a is the activation energy, and α is the alkali concentration index. Environmental compliance rules are quantified through the chemical oxygen demand emission constraint equation:

$$\mathrm{COD}_{\mathrm{pred}}=\sum_{i=1}^{n}\left(\frac{C_i\cdot M_i}{\rho_i}\cdot\delta_i\right)+\beta\cdot V_w \tag{3}$$

In Formula 3, C_i is the concentration of the i-th additive, M_i is its molecular weight, ρ_i is the density, δ_i is the biodegradation coefficient, V_w is the washing volume, and β is the baseline coefficient of process water.

The GraphSAGE mean aggregator is used for graph embedding representation learning, and the neighborhood features of each dye node v are aggregated:

$$\mathrm{h}_v^{(l)}=\mathrm{ReLU}\left(W^{(\mathrm{l})}\cdot\mathrm{MEAN}_{u\in N(v)}\left(\mathrm{h}_u^{(l\text{-}1)}\right)\right) \tag{4}$$

In Formula 4, $N(v)$ is the neighborhood set of node v, $W^{(l)}$ is the trainable parameter matrix of the l layer, and the activation function ReLU (Rectified Linear Unit) ensures nonlinear feature extraction.

Dynamic Process Time Series Data Acquisition

During the steam fixation and water washing process, a distributed fiber Bragg grating sensor network is deployed to monitor real-time changes in process parameters, and an IEPE (Integrated Electronic Piezoelectric) piezoelectric flowmeter records the instantaneous flow $Q(t)$ of the water washing unit.

According to the fixation kinetics of reactive dyes, the steam temperature–time coupling feature matrix is constructed:

$$\mathbf{X}_{\text{temp}}=\begin{bmatrix} T_1(t_1) & T_1(t_2) & \cdots & T_1(t_n) \\ T_2(t_1) & T_2(t_2) & \cdots & T_2(t_n) \\ \vdots & \vdots & \ddots & \vdots \\ T_m(t_1) & T_m(t_2) & \cdots & T_m(t_n) \end{bmatrix} \tag{5}$$

In Formula 5, $T_i(t_j)$ represents the measured temperature of the i temperature zone at time t_j, m is the number of temperature zones, and n is the total number of time sequence steps.

The dynamic effect of water washing intensity is quantified by the cumulative flow–time integral equation:

$$W_{\text{total}}=\int_0^{t_{\text{wash}}} Q(t)\cdot\eta_p dt \tag{6}$$

In Formula 6, $Q(t)$ is the instantaneous flow rate, η_p is the pumping efficiency coefficient, and t_{wash} is the water washing cycle. Combined with the wastewater ion concentration $C_{ion,i}(t)$ measured by the conductivity sensor, a dynamic COD correction model is established:

$$\text{COD}(t)=\alpha_1\cdot\sum_{i=1}^{k}\left(\frac{dQ_i}{dt}\cdot C_{\text{ion},i}(t)\right)+\beta_1\cdot\frac{dW_{\text{total}}}{dt} \tag{7}$$

In Formula 7, α_1 and β_1 are empirical calibration coefficients, and k is the number of washing units.

This method synchronizes process parameters such as temperature, flow, and conductivity to a unified time base, improves temporal resolution, and provides high-precision dynamic feature input for the BiLSTM layer.

GraphSAGE-BiLSTM Fusion Model Design

The GraphSAGE layer extracts the neighborhood chemical compatibility characteristics of the dye node through the mean aggregator, and the BiLSTM layer uses a dual-gated unit to decode the temporal dynamics of the evaporation–washing process, ultimately achieving cross-modal feature weight allocation through the attention mechanism. Node features are defined as follows: Reactive Dye nodes are encoded with their molecular weight, sulfonic acid group count, and Zeta potential; Color Fixative nodes are encoded with their charge type (cationic/anionic), molecular structure, and reactivity; Fiber Substrate nodes are characterized by material type and surface properties. Edges are constructed based on domain rules: "Chemical Compatibility" edges connect dyes to fixatives, with weights derived from the ionic electrical matching model; "Process Impact" edges link parameters to processes, weighted by empirical sensitivity coefficients; "Environmental Compliance" edges enforce regulatory constraints. In the GraphSAGE propagation stage, the adjacent auxiliary agent set of each reactive dye node is embedded in multiple layers:

$$h_v^{(l)}=\mathrm{ReLU}\left(W^{(l)}\cdot\left[\mathrm{MEAN}_{u\in N(v)}\left(h_u^{(l-1)}\right)\,//\,h_v^{(l-1)}\right]\right) \tag{8}$$

In Formula 8, // represents the vector concatenation operation, $W^{(l)}$ is the trainable parameter matrix of the l layer, $h_v^{(l-1)}$ is the current representation of node v, and $h_u^{(l-1)}$ is the low-dimensional feature of the adjacent auxiliary node. The dye–auxiliary compatibility feature matrix $H_{graph}\in R^{d\times 128}$ is then output.

The BiLSTM layer uses forward and reverse LSTM networks to process the evaporation temperature curve and water washing flow sequence in parallel:

$$\vec{h}_t=\overrightarrow{\mathrm{LSTM}}\left(\mathbf{x}_t,\vec{h}_{t-1}\right),\ \overleftarrow{h}_t=\overleftarrow{\mathrm{LSTM}}\left(\mathbf{x}_t,\overleftarrow{h}_{t+1}\right) \tag{9}$$

In Formula 9, x_t is the process parameter input vector at time t, and the memory cell state is controlled by the gate unit.

The multi-head attention mechanism is used to dynamically allocate weights in the feature fusion stage:

$$\text{Attention}(\mathbf{Q},\mathbf{K},\mathbf{V})=\text{softmax}\left(\frac{\mathbf{Q}\mathbf{K}^T}{\sqrt{d_k}}\right)\mathbf{V} \tag{10}$$

In Formula 10, the query matrix $Q\in R^{d\times d_k}$ is generated by the GraphSAGE embedding features, and the key matrix $K\in R^{2n\times d_k}$ and value matrix $V\in R^{2n\times d_v}$ come from the BiLSTM hidden state. The calculation is performed through eight parallel attention heads:

$$\begin{aligned}&\text{MultiHead}=\text{Concat}(\text{head}_1,\ldots,\text{head}_h)W^O\\&\text{head}_i=\text{Attention}(\mathbf{H}_{\text{graph}}W_i^Q,\mathbf{H}_{\text{lstm}}W_i^K,\mathbf{H}_{\text{lstm}}W_i^V)\end{aligned} \tag{11}$$

Finally, the fusion feature $Z\in R^{d\times 512}$ is finally input into the fully connected layer, and the predicted values for color fastness to washing $\hat{F}$ and color difference ΔE are output:

$$\hat{F}=\text{Sigmoid}\left(W_f\mathbf{Z}+b_f\right),\ \Delta E=\left\|W_e\mathbf{Z}+b_e\right\|_2 \tag{12}$$

This design achieves joint optimization of the color penetration rate in the ink gradient area and the co-hydrolysis reaction intensity of the high-saturation color block through collaborative modeling of chemical compatibility constraints and process timing effects.

Multi-objective Process Parameter Optimization

Based on the model's output predictions, a multi-objective optimization problem is constructed with five objective functions: minimizing color difference ΔE, the color penetration rate ρ_{bleed} in the ink gradient area, COD emission, and additive amount of additives C_{add}, while maximizing color fastness to washing F. Optimization variables include the evaporation temperature gradient, water washing flow rate, color fixative concentration, and process time, with their value ranges constrained by the process influence weight matrix in the knowledge graph:

$$\begin{gathered} min\left[\Delta E=/\!/ W_e\mathbf{Z}+b_e /\!/ _2, \rho_{\text{bleed}}=\frac{A_{\text{diffuse}}}{A_{\text{original}}}\right] \\ max\left[F=\text{Sigmoid}\left(W_f\mathbf{Z}+b_f\right)\right] \\ min\left[\text{COD}_{\text{pred}}=\sum_{i=1}^{n}\left(\frac{C_iM_i}{\rho_i}\delta_i\right)+\beta V_w, C_{\text{add}}=\sum_{j=1}^{m} C_j\right] \end{gathered} \tag{13}$$

In Formula 13, $Z\in R^{d\times 512}$ is the fusion feature matrix, $A_{diffuse}$ and $A_{original}$ are the grayscale area integral values of the bleeding area and the original pattern, respectively. The process constraint is embedded in the objective function via a penalty function:

$$\Phi(\mathbf{x})=f(\mathbf{x})+\lambda_1 max(0,\varepsilon_{ij}-0.3)+\lambda_2 max(0,\text{COD}_{\text{pred}}-\text{COD}_{\text{max}}) \tag{14}$$

In Formula 14, λ_1,λ_2 are penalty coefficients, ε_{ij} is the electrical matching degree of dyes and auxiliary agents, and COD_{max} is the emission limit. This design ensures the solution set strictly meets the ion electrical conflict warning mechanism and environmental compliance rules. The optimal compromise solution is determined by fuzzy set theory:

$$\mu_k=\frac{\prod_{i=1}^{5}\left(1-\frac{d_{ik}}{D_i}\right)}{\sum_{j=1}^{200}\prod_{i=1}^{5}\left(1-\frac{d_{ij}}{D_i}\right)}\ (k=1,2,\ldots,200) \tag{15}$$

In Formula 15, d_{ik} is the normalized deviation of the i target at solution k, and D_i is the maximum allowable deviation (i.e., normalized boundary value) of the i target. When $d_{ik}=0$, solution k reaches the ideal value for target i; when $d_{ik}=D_i$, it means that solution k reaches the process acceptable boundary value for target i, and the membership degree of the target drops to 0. The solution corresponding to the maximum membership μ_k is selected as the recommended solution for industrialization, achieving a multi-dimensional balance among color fastness improvement, color bleeding suppression, and green production.

EXPERIMENTAL DESIGN

This paper uses a 55/45 silk/cotton blended base fabric as the carrier and selects typical Chinese garden-style patterns containing ink-colored gradient rocks, high-saturation cinnabar-colored peonies, and fine indigo

pavilion outlines for process verification. For cultural characteristic elements, a special detection method is used: the ink-colored gradient area is measured by microscopic imaging, the cinnabar color block is monitored with a spectrophotometer for CIELAB color space *a** value and chromaticity angle, and the pavilion outline is quantified by an edge sharpness algorithm. These objective measurements directly relate to the core aesthetic principles of Chinese garden art. Microscopic imaging of gradient areas quantifies the "flying white" effect, a hallmark of traditional ink painting. The CIELAB *a** value and chromatic angle of the cinnabar color patch ensure color adherence to traditional principles—a higher *a** value indicates a more vibrant and realistic vermilion. Edge sharpness reflects the clarity of fine brushwork, and increased contrast directly reflects enhanced visual depth and artistic expression.

To reveal the unique process sensitivity of garden fabrics compared to traditional printing, this paper designed a parameter sensitivity analysis experiment. On the same substrate, 32 batches of process data were collected; both garden-style patterns and traditional geometric printing were applied; the evaporation temperature gradient and water washing flow were systematically varied; and the response slope differences in ΔE, color penetration rate, and edge sharpness were compared and analyzed. An L9(3^4) orthogonal test design was used to optimize key process parameters—evaporation temperature, steaming time, washing flow rate, and fixative dosage—for a specific dye–fixative combination, generating nine high-quality experimental datasets. Additional data from five other dye–fixative combinations under standard processes were included, forming a comprehensive benchmark dataset for model training. This dataset was then used to train and validate the GraphSAGE-BiLSTM fusion model as well as several baseline models. The performance of the proposed GraphSAGE-BiLSTM model, when applied to generate new process parameters, was subsequently evaluated against results from the original orthogonal test method. The industrial production line covers key parameter ranges, such as evaporation temperature gradient, water washing flow, and six dye–fixing agent combinations; to address the challenge of small samples, the Mixup strategy was used to expand the training data to three times the original. The Mixup data augmentation strategy is applied to the high-dimensional process feature vectors extracted by the BiLSTM encoder, rather than the raw time-series sensor data, ensuring that the generated samples maintain physical plausibility. Finally, a multi-source heterogeneous database containing multiple quality inspection indicators is established.

The optimized process plan output by the model is verified on the industrial production line after the Pareto frontier is solved by the NSGA-II algorithm. Experimental comparison plans include: the experimental group adopting the complete GraphSAGE-BiLSTM optimization plan; the control group continuing to use the

orthogonal test benchmark parameters. The control group is based on a standard L9(3^4) orthogonal design, with benchmark parameters set at an evaporation temperature of 103°C, a steaming time of 7 minutes, and a washing flow rate of 25 L/min, representing the factory's current standard operating procedure; the control group G-only (GraphSAGE optimization only) ignores timing dynamics; the control group B-only (BiLSTM optimization only) ignores compatibility rules. The experimental plan also includes the fusion architecture of graph attention network and temporal convolutional network GAT-Graph Attention Network + TCN (Temporal Convolutional Network) and a multi-task Transformer model. Quality inspection strictly follows ISO 105-C06 standard, combining spectrophotometer, microscopic imaging, and Hach COD analyzer, and verifies significant differences between the experimental and control groups in cultural characteristic indicators, color quality, environmental protection, and cost using double sample tests, forming a closed-loop verification process.

MODEL TRAINING AND EVALUATION

Model Training and Loss Function

During model training, the model uses the 128-dimensional embedding vector of the knowledge graph as static input, the evaporation temperature gradient and washing flow time series as dynamic input, and supervision signals including washing color fastness grade, color difference ΔE, color penetration rate, and COD emissions. The latent space feature distance between the pattern and the design draft is calculated through a pre-trained StyleGAN2 model as a quantitative indicator of aesthetic consistency. The Adam optimizer is used for end-to-end training, and the loss function integrates L1 loss, cross-entropy loss, and mean square error:

$$L=\alpha\cdot L_{L1}(\Delta E)+\beta\cdot L_{CE}(F)+\gamma\cdot L_{MSE}\left(\rho_{\text{bleed}}\right) \quad (16)$$

In Formula 16, $\alpha = 0.4$, $\beta = 0.3$, $\gamma = 0.3$, corresponding to the L1 loss of color difference, the cross-entropy loss of color fastness, and the mean square error of color bleeding rate. The dynamic weight mechanism adjusts the optimization focus according to the process stage: the steaming stage focuses on color fastness and hydrolysis control, while the washing stage focuses on color bleeding suppression. The training and test sets are divided in an 8:2 ratio, and the early stopping strategy is adopted (validation loss terminates after 15

rounds without improvement). To prevent data leakage in time series prediction, the dataset was split chronologically: the earliest 80% of sequential process records were used for training/validation, and the most recent 20% were reserved for testing. Model parameter initialization is shown in Table 1.

Table 1. Model parameter initialization table

Parameter Category	Parameter name	Initialization method	Numerical range
GraphSAGE layer	Neighbor Sampling Size	Fixed value	10
	Weight matrix $W^{(1)}$	Xavier uniform distribution	[-0.062, 0.062]
	Weight matrix $W^{(2)}$	Xavier uniform distribution	[-0.044, 0.044]
	Activation Function	Fixed	ReLU
BiLSTM layer	Hidden layer dimension (Forward/Reverse)	Fixed value	64
	Gating Unit Weight Initialization	Xavier uniform distribution	[-0.125, 0.125]
	Memory Cell Initial State	Fixed	Zero Vector
Attention mechanism	Number of heads	Fixed value	8
	Key Matrix Dimension d_k	Fixed value	64
Optimizer	Initial learning rate	Exponential decay scheduler	1×10^{-3}
	Weight decay coefficient	Fixed	1×10^{-4}
Task loss weights	Color Difference Loss Coefficient α	Analytic Hierarchy Process	0.4
	Color Fastness Loss Coefficient β	Fixed	0.3
	Bleeding Rate Loss Coefficient γ	Fixed	0.3

Evaluation Indicators

This study uses core color stability indicators and industrial engineering performance indicators to evaluate the optimization effect and deployment feasibility of the model.

Color stability indicators include color difference ΔE, reflecting the color deviation between the printed fabric and the design draft, according to the CIEDE2000 color difference standard. Washing color fastness F is tested according to ISO 105-C06 standard, with color retention ability quantified by gray sample rating; results are reported on a standard 1–5 grade scale, where 5 indicates no color change and 1 indicates severe fading. The color penetration rate in the ink gradient area is ρ_{bleed}.

COD emissions are measured directly by a Hach DR3900 laboratory analyzer, calculated based on the absorbance linear regression model of the potassium dichromate oxidation reaction. Process cost statistics comprise the sum of the amount of additives and energy consumption per unit area.

In industrial deployment, inference delay represents the time taken to optimize a single batch; memory usage is the resident memory after the model is loaded; process stability is the fluctuation range of recommended process parameters over 32 batches of continuous production, quantified by the standard deviation of the evaporation temperature gradient. Process stability is quantified by the standard deviation of the evaporation temperature gradient, as this parameter is the most sensitive control variable affecting dye fixation and color stability during the steaming process. A lower standard deviation indicates a more robust and repeatable process.

The above indicators constitute the supervision signal for multi-objective optimization, with network parameters updated by backpropagation of the error between the model prediction and measured values, ultimately achieving coordinated optimization of color stability, environmental protection, and economy.

VERIFICATION OF THE OPTIMIZATION EFFECT OF COLOR STABILITY IN CHINESE GARDEN-STYLE FABRICS

Embedding Effect of Domain Rules in Dyeing and Finishing Knowledge Graph

To verify the modeling ability of the graph for compatibility constraints, the matching degree of GraphSAGE prediction and manual experience rules was compared. Six dye–auxiliary combinations—Dye1-M30, Dye2-M30, Dye3-DSD acid, Dye4-cation A, Dye5-nonionic B, Dye6-anionic C—were selected for the experiment. Each group contains predicted values, calibration values, and conflict warning states. The comparison results are shown in Figure 2.

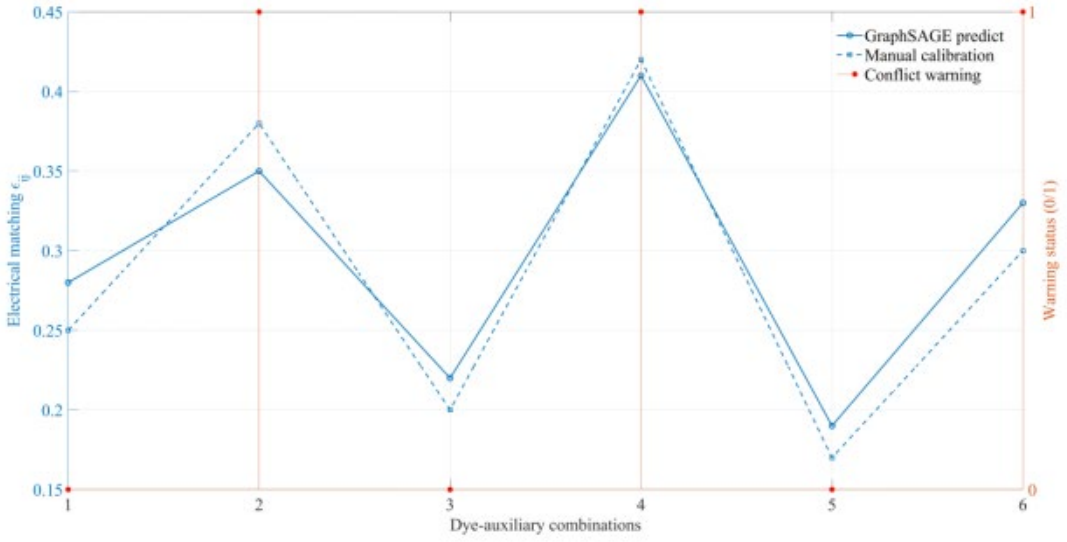

Figure 2. Comparison between GraphSAGE prediction and manual rules

Figure 2 presents the comparison between the GraphSAGE model's predictions for the electrical matching of dyes and auxiliary agents and the calibration values of manual experience rules, as well as the corresponding conflict warning status. The horizontal axis represents six different dye–auxiliary combinations, numbered 1 to 6; the left vertical axis represents the electrical matching; and the right vertical axis represents the binary state of conflict warning (0 is no warning, 1 is triggered warning). The data show that the trend of GraphSAGE prediction values is consistent with manual calibration values. The predicted ε_{ij} for combination Dye1 is 0.28, and the calibration value is 0.25; both are below the threshold of 0.3 and do not trigger a warning. The predicted value for combination Dye2 is 0.35, and the calibration value is 0.38; both exceed 0.3, resulting in activation of the conflict warning. The warning status of all combinations fully complies with rule constraints. The results demonstrate that the GraphSAGE model accurately captures the ionic electrical matching characteristics between dyes and auxiliaries, verifying the effectiveness of chemical compatibility constraint modeling in the knowledge graph. Additionally, the early warning distribution reveals that combinations with cationic/high-charge additives are prone to electrical conflicts, providing key constraints for multi-objective optimization and supporting subsequent processes to synergistically improve color fastness and environmental protection while avoiding conflicts.

Dynamic Modeling Accuracy Analysis of Timing Process Parameters

To verify the dynamic modeling capability of timing process parameters, the prediction error of BiLSTM on

the evaporation temperature curve and dye fixation rate is analyzed, with the error of dye fixation rate in the evaporation stage predicted by BiLSTM. The comparison results are shown in Figure 3.

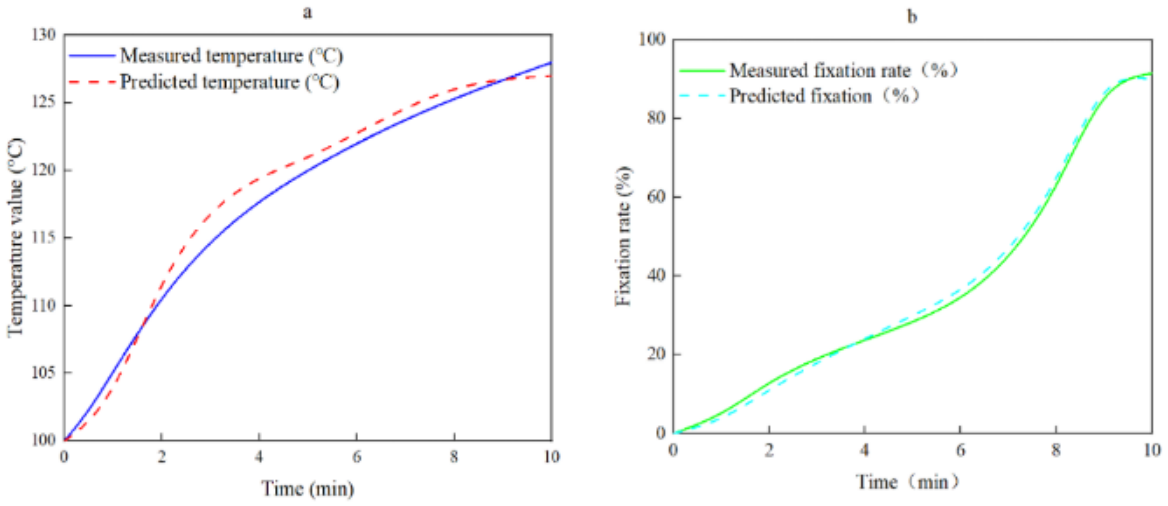

Figure 3. BiLSTM prediction accuracy of evaporation temperature and fixation rate. (a) Evaporation temperature change curve over time; (b) Curve of dye fixation rate over time

Figure 3 shows the prediction accuracy of the evaporation temperature curve and fixation rate. Data in subfigure (a) show the predicted value is lower than the measured value during the initial 1–2 minutes, higher than the measured value in the middle period, and gradually converges to 127.0°C in the final 9–10 minutes, when the measured value reaches 128.0°C. Data in subfigure (b) indicate that the difference between the measured fixation rate curve and the predicted curve is more pronounced in the middle period: the predicted value of 11.0% at 2 minutes is lower than the measured value of 12.8%, with an error of –1.8%; the predicted value of 65.0% at 8 minutes is higher than the measured value of 63.2%, with an error of +1.8%; and the error is reduced to 1.5% at 10 minutes. The difference between the two reflects the temporal cumulative effect of the hydrolysis reaction of the reactive dye.

The data trends verify the high-precision modeling capability of GraphSAGE-BiLSTM for temporal dynamics. This accuracy stems from the synergistic mechanism of GraphSAGE's quantitative compatibility rules and BiLSTM's decoding of timing, effectively capturing the cumulative effect of hydrolysis reactions, with robustness meeting engineering requirements. This capability directly supports the improvement of color stability in multi-objective optimization and enables industrial closed-loop control.

Comparison of Color Stability Optimization Results

To verify the optimization effect on color stability in the dyeing and finishing process, the experimental group using the GraphSAGE-BiLSTM optimization scheme and recommended process parameters was compared with the control group using the traditional orthogonal experimental method. The comparison results are shown in Figure 4.

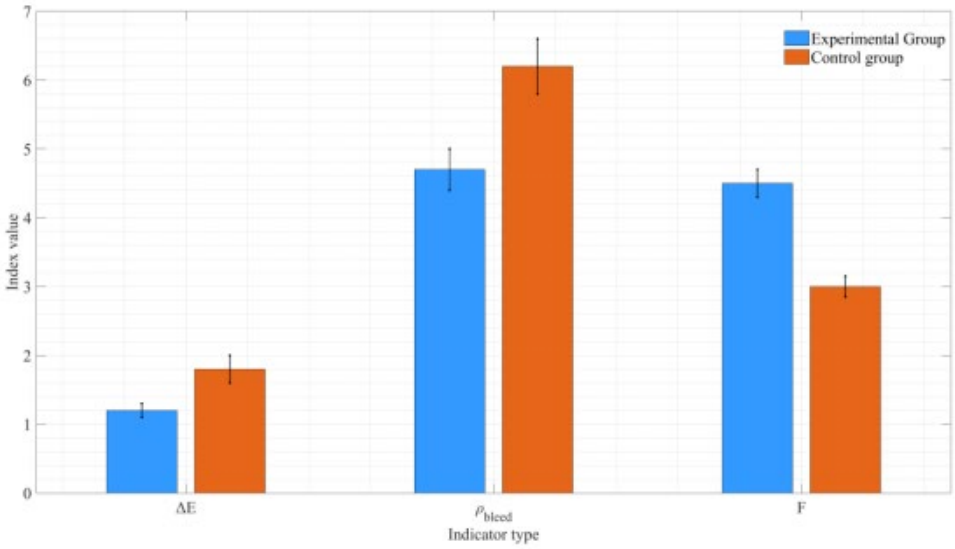

Figure 4. Comparison of core color stability indicators

Figure 4 presents the comparison results of core color stability indicators between the experimental group and the traditional orthogonal test control group. The horizontal axis represents three key indicators. The data show significant advantages for the experimental group over the orthogonal test method: color difference (ΔE) is reduced by 33.3% compared with the control group (from 1.8), minimizing color deviation between the printed fabric and the design draft; color penetration rate is reduced from 6.2% to 4.7%, a reduction of 1.5%, indicating effective suppression of dye migration in the ink gradient area; and color fastness to washing is increased by 50%, greatly improving color stability during washing. The error bars further verify the robustness of the optimization scheme.

This improvement is due to the synergistic mechanism of GraphSAGE-BiLSTM: the knowledge graph quantifies compatibility constraints (such as electrical matching), BiLSTM decodes evaporation–washing time series dynamics, and NSGA-II achieves Pareto optimality. This method not only meets the stringent requirements of

garden style (ink gradient/high-saturation color blocks/fine contours), but also realizes industrial application through energy saving and reduced consumption.

Process Cost and Environmental Protection Analysis

To verify the industrial feasibility of the scheme, the experiment was divided into four groups according to process parameters: group A (low intensity), group B (medium intensity), group C (high intensity), and the experimental group. Feasibility and sustainability of industrialization were analyzed by comparing environmental protection indicators such as additive usage and energy consumption of water washing in each process parameter group. The comparison results are shown in Figure 5.

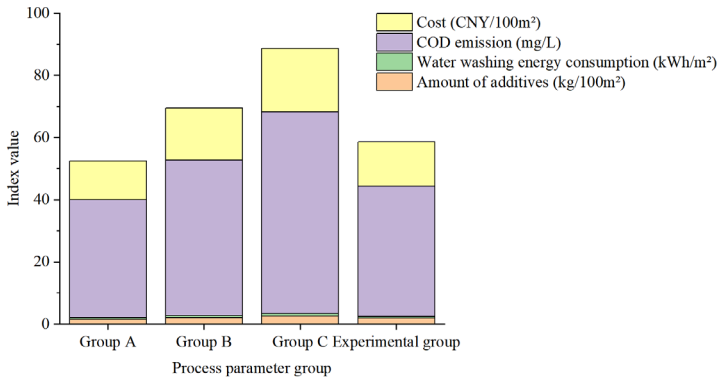

Figure 5. Comparison of process cost and environmental performance

Figure 5 presents a comprehensive comparison of four different process parameter groups regarding process cost and environmental performance indicators. The values cover four indicators: additive dosage (kg/100 m²), water washing energy consumption (kWh/m²), COD emissions (mg/L), and cost (CNY/100 m²). The data show that the experimental group's additive amount is reduced by 10% compared with group B, water washing energy consumption is reduced by 14.5%, COD emissions are reduced by 16%, and cost is reduced by 15.5%. As process intensity increases from low to high (Group A to Group C), all four indicators exhibit linear growth, with Group C showing the highest COD emission (65 mg/L) and cost (20.3 CNY/100 m²), reflecting the positive correlation between resource input and environmental pressure in traditional processes. The changes indicate that the experimental group maintains processing capacity similar to the medium-intensity process while reducing resource consumption and environmental burden, overcoming the inherent contradiction of increased cost and pollution caused by increased intensity in traditional processes.

Coordinated optimization of process parameters was achieved: reliance on high-cost auxiliaries was reduced, and energy consumption and wastewater pollution were lowered by dynamically adjusting washing intensity. Ultimately, a balance between economy and environmental protection was found on the Pareto frontier, verifying the industrial feasibility of the solution and providing a reusable technical paradigm for green manufacturing in the textile industry.

Verification of Detail Preservation of Complex Patterns

To verify the detail preservation ability of complex patterns in Chinese garden-style fabrics using the GraphSAGE-BiLSTM model, the experiment compared detail preservation in three pattern areas—ink gradient area, pavilion outline, and cinnabar peony—with the orthogonal test method control group. The comparison results are shown in Figure 6.

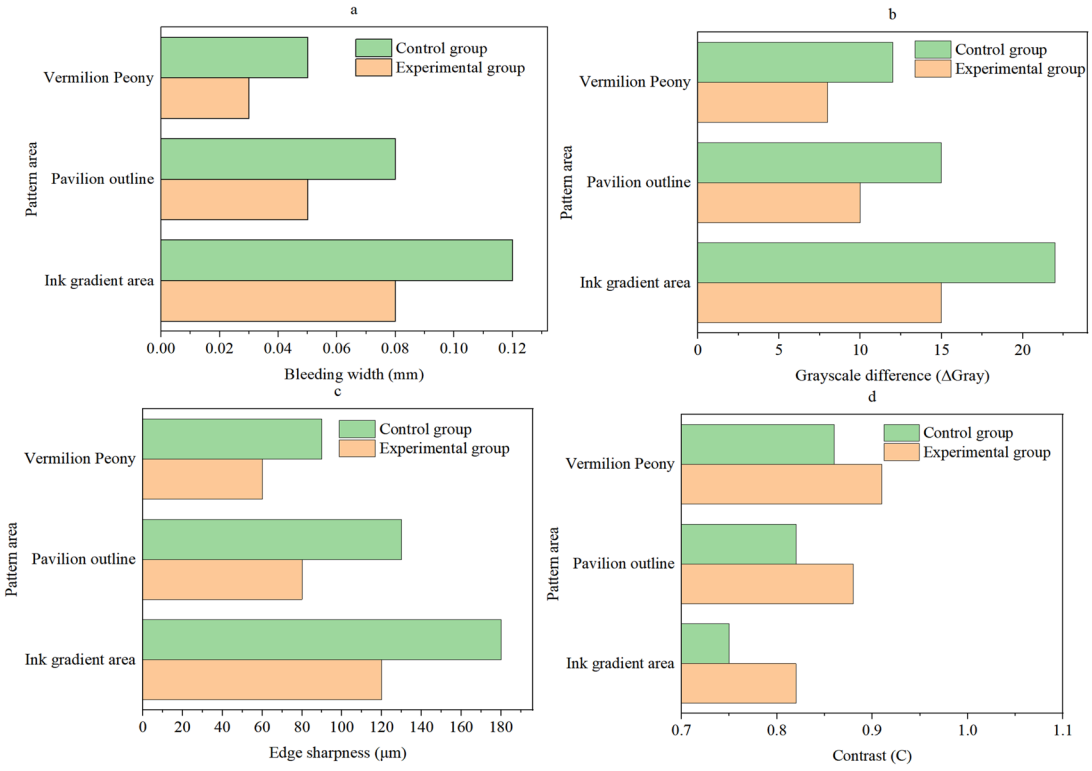

Figure 6. Comparison of detail preservation in various indicators of complex patterns. (a) Color bleeding width comparison; (b) Grayscale difference comparison; (c) Edge sharpness comparison; (d) Contrast comparison

Figure 6 presents the comparison results for color bleeding width, grayscale difference, edge sharpness, and contrast in different pattern areas based on the GraphSAGE-BiLSTM optimization framework. The reduction

in color bleeding width indicates effective suppression of dye migration, especially in the cinnabar peony area, where the experimental group reaches the lowest value of 0.03 mm and the control group is at 0.05 mm, demonstrating the model's strongest protection for highly saturated color blocks. The reduction in grayscale difference reflects clearer pattern edges, avoiding ink smudge; optimized edge sharpness directly reflects the protective effect on fine contours, ensuring the integrity of the pavilion structure in the garden style. The improvement in contrast compared to the control group indicates clearer color levels, reaching 0.82 in the ink gradient area, which is 0.07 higher than the control group.

These changes intuitively verify the collaborative optimization capability of the GraphSAGE-BiLSTM framework, ultimately achieving Pareto optimal solutions driven by a multi-objective genetic algorithm. This not only meets the stringent requirements of Chinese garden-style fabrics for ink gradients, highly saturated color blocks, and fine patterns, but also considers industrial feasibility, providing a reusable technical paradigm for optimizing the color stability of cultural and creative textiles.

Comparison of Optimization Effects of Different Models

To evaluate the performance of the GraphSAGE-BiLSTM fusion model proposed in this paper, six comparison schemes were established, focusing on dual-dimensional performance verification of traditional color quality indicators and industrial engineering indicators. The indicator results of 32 batches of tests on 55/45 silk/cotton blended base fabrics for each model are shown in Table 2.

Table 2. Comparative analysis of multi-model color quality and industrial engineering indicators

Index	Control	G-only	B-only	GAT+TCN	Transformer	Proposed
Color Difference ΔE	1.80 ± 0.20	1.55 ± 0.18	1.62 ± 0.17	1.48 ± 0.16	1.65 ± 0.19	1.20 ± 0.10
Color Fastness to Washing F (grade)	3.0 ± 0.15	3.8 ± 0.20	3.5 ± 0.18	4.0 ± 0.22	3.7 ± 0.20	4.5 ± 0.2
Color Penetration Rate (%)	6.2 ± 0.4	5.3 ± 0.3	5.8 ± 0.4	5.0 ± 0.3	5.5 ± 0.4	4.7 ± 0.3
COD Emission (mg/L)	65 ± 5	58 ± 4	62 ± 5	55 ± 4	60 ± 5	42 ± 3
Inference Latency (ms)	–	18 ± 2	20 ± 2	15 ± 1	45 ± 5	22 ± 2
Memory Usage (MB)	–	280	310	260	420	350
Process Stability	0.12 ± 0.02	0.08 ± 0.01	0.10 ± 0.01	0.07 ± 0.01	0.11 ± 0.02	0.05 ± 0.01

As shown in Table 2, the GraphSAGE-BiLSTM fusion model proposed in this study achieves a breakthrough in solving the color stability problem of Chinese garden-style fabrics. The key indicator ΔE is reduced to 1.20, which is 33.3% lower than the 1.80 of the traditional orthogonal method (Control). Color fastness to washing reaches level 4.5, color penetration rate is optimized to 4.7%, and COD emission is reduced to 42 mg/L. At the industrial level, the 22 ms inference delay meets the real-time control requirements of the production line, and the 0.05 process stability ensures production reliability. This inference speed is achieved on an NVIDIA Jetson AGX Xavier edge device with a compressed model size of 8.7 MB and a batch size of 1, after input preprocessing (sensor data synchronization and normalization), ensuring real-time performance for online process control. The comparison shows that although the GAT+TCN model has lower latency, its ΔE of 1.48 and color penetration rate of 5% lag behind the model proposed in this paper; the Transformer model has a high latency of 45 ms, which reduces its industrial feasibility. The proposed model integrates dye matching rules and temporal dynamic decoding to achieve dual-objective optimization of cultural expression and industrial production while protecting the artistic characteristics of garden fabrics.

The computational burden of the proposed method was evaluated against the traditional orthogonal test (Control). While offline training of the GraphSAGE-BiLSTM model requires approximately 4 hours on an NVIDIA A100 GPU, this is a one-time cost. Despite higher initial computational cost, the AI-driven approach effectively reduces time and resource consumption compared to the labor-intensive traditional method, making it highly suitable for industrial deployment.

DISCUSSION OF LIMITATIONS

The model's generalization ability is currently limited by the use of a single silk/cotton blend substrate and a finite data collection cycle. Its performance on multi-component fibers or under extreme process conditions requires further validation. Future work will expand the dataset and explore transfer learning to address this limitation. Nonetheless, the integration of chemical rules with temporal dynamics offers a novel methodological framework that demonstrates potential for broader application in industrial textile optimization.

CONCLUSIONS

This study presents a novel GraphSAGE-BiLSTM framework for collaborative optimization of dyeing and finishing processes in Chinese garden-style printed fabrics. The core contribution lies in its ability to synergistically model structured chemical rules and temporal process dynamics, a critical gap in existing methodologies. By integrating a knowledge graph to quantify dye–auxiliary compatibility constraints and a BiLSTM network to decode the steaming–washing time series, the framework successfully drives a multi-objective optimization process that achieves a Pareto-optimal balance between aesthetic fidelity and industrial efficiency. Our work demonstrates that the future of textile process optimization lies not in isolated parameter tuning, but in holistic integration of domain knowledge and data-driven modeling. The achieved improvements—such as a 33.3% reduction in color difference and a 10–15% reduction in resource consumption—are not merely incremental gains, but evidence of a paradigm shift toward intelligent, closed-loop manufacturing. This research provides a novel methodological framework for optimizing the color stability of cultural and creative textiles, with broad implications for enhancing the industrialization of traditional crafts while preserving their artistic essence. The innovation lies in overcoming the bottleneck of integrating structured rules (electrical conflict warning/hydrolysis kinetics) and time series modeling, laying the groundwork for future development in this domain. Limited by the experimental data collection cycle and the singularity of the textile substrate, the model's generalization ability for multi-component fiber adaptability and extreme process conditions still needs to be expanded.

Author Contributions

All work in this study was independently completed by Lin ZHOU.

Conflicts of Interest

The author declares no conflict of interest.

Funding

This research was funded by the 2024 National Social Science Fund Art Studies Project "Research on the Design of Chinese Gardens Overseas" (No. 24BG134).

Acknowledgements

Not applicable.

REFERENCES

[1] Li Y, Huang Y, Yang L, Zhang X, Zhang R. Study on color ink diffusion in fabrics and color reproduction of digital inkjet printing. Textile Research Journal. 2022; 92(19-20):3733-3749. doi: 10.1177/00405175221094046

[2] Vodyashkin AA, Makeev MO, Mikhalev PA. Inkjet Printing Is a Promising Method of Dyeing Polymer Textile Materials. Polymers. 2025; 17(6):756. doi: 10.3390/polym17060756

[3] Li L, Chu R, Yang Q, Li M, Xing T, Chen G. Performance of Washing-Free Printing of Disperse Dye Inks: Influence of Water-Borne Polymers. Polymers. 2022; 14(20):4277. doi: 10.3390/polym14204277

[4] Ragab M, Hassabo A, Othman H. An Overview of Natural Dyes Extraction Techniques for Valuable Utilization on Textile Fabrics. Journal of Textiles, Coloration and Polymer Science. 2022; 19(2):137-153. doi: 10.21608/jtcps.2022.130253.1115

[5] Zhang C, Zhao X, Hu Z, Liu J, Zheng S, Tang W, et al. Hydrolyzed Reactive Red 195 adsorption on cellulose: Experimental and theoretical investigations. Journal of Engineered Fibers and Fabrics. 2024; 19. doi: 10.1177/1558925023122346

[6] Hernández V, Galleguillos F, Sagredo N, Machuca, Á. Color fastness of fabrics after dyeing with fungal dyes. International Journal of Clothing Science and Technology. 2021; 33(2):232-240. doi: 10.1108/IJCST-12-2019-0196

[7] Rainert KT, de Oliveira CRS, Felipe BHS, Herpich H, Valle Rita de Cássia Siqueira Curto, Valle JAB. Textile printing: An integrated view of processes, properties, and future prospects. Coloration Technology. 2024; 140(4):556-570. doi: 10.1111/cote.12746

[8] Liang L, Li H, Cai X, Dai Y, Yan J. Enhancing the outline sharpness of crosslinked printed cotton fabrics using ethylene glycol diglycidyl ether. Coloration Technology. 2024; 140(2):270-278. doi: 10.1111/cote.12709

[9] Kalayci E, Avinc O. The Disperse Dyeing of Polyetherimide Fibers Using Orthogonal Array (Taguchi) Design. Fibers and Polymers. 2024; 25(8):3045-3060. doi: 10.1007/s12221-024-00641-1

[10] Pervez MN, Yeo WS, Lin L, Xiong X, Naddeo V, Cai Y. Optimization and prediction of the cotton fabric dyeing process using Taguchi design-integrated machine learning approach. Scientific Reports. 2023; 13(1):12363. doi: 10.1038/s41598-023-39528-1

[11] Neral B, Gorgieva S, Kurečič M. Decontamination Efficiency of Thermal, Photothermal, Microwave, and Steam Treatments for Biocontaminated Household Textiles. Molecules. 2022; 27(12):3667. doi: 10.3390/molecules27123667

[12] He Z, Xu J, Tran KP, Thomassey S, Zeng X, Yi C. Modeling of textile manufacturing processes using intelligent techniques: a review. The International Journal of Advanced Manufacturing Technology. 2021; 116(1):39-67. doi: 10.1007/s00170-021-07444-1

[13] Paranjape M, Athalye A. Cationic Surfactants in Textile Processing. Indian Journal of Fibre and Textile Engineering (IJFTE). 2025; 5(1):15-23. doi: 10.54105/ijfte.A2419.05010325

[14] Barros SM, Andrade RS, Torres D, Chiari-Andreo BG, Veloso GB, Gonzalez C, et al. Eco-Friendly Technology for Reactive Dyeing of Cationized Fabrics: Protic Ionic Liquids as Innovative Media. Cellulose Chemistry and Technology. 2022; 56(3-4):403-425. doi: 10.35812/CelluloseChemTechnol.2022.56.36

[15] Uğur ŞS. Sustainable Dyeing and Finishing of Cotton Fabrics with Layer-by-Layer Technique. Coatings. 2023; 13(6):1129. doi: 10.3390/coatings13061129

[16] Liang Y, Wang N, Li Q, Jiang H. Surface Modification of Silk Fabric by Polysaccharide Derivatives towards High-Quality Printing Performance Using Bio-Based Gardenia Blue Ink. Materials. 2024; 17(14):3611. doi: 10.3390/ma17143611

[17] Rahayuningsih E, Marfitania T, Pamungkas MS, Fatimah WS. Optimization of cotton fabrics dyeing process using various natural dye extracts. Jurnal Rekayasa Proses. 2022; 16(1):58-65. doi: 10.22146/jrekpros.70397

[18] Repon MR, Islam T, Paul TK, Jurkonienė S, Haji A, Shukhratov S, et al. Natural dyes in textile printing: Parameters, methods, and performance. Environmental Science and Pollution Research. 2024; 31(35):47552-47583. doi: 10.1007/s11356-024-34424-1

[19] Ömeroğulları Z. Coloring Cotton Fabrics by Pigment Printing Method with Reduction of Process Steps: An Innovative Approach. Duzce University Journal of Science and Technology. 2025; 13(2):643-654. doi: 10.29130/dubited.1589566

[20] Ingle N, Jasper WJ. A review of deep learning and artificial intelligence in dyeing, printing and finishing. Textile Research Journal. 2025; 95(5-6):625-657. doi: 10.1177/00405175241268619

[21] Liang J, Zhou J, Hu X, Luo H, Cao G, Liu L, et al. Digital Grading the Color Fastness to Rubbing of Fabrics Based on Spectral Reconstruction and BP Neural Network. Journal of Imaging. 2023; 9(11):251. doi: 10.3390/jimaging9110251

[22] Şahin C, Balcı O, Işık M, Gökenç İ. Artificial neural networks approach for prediction of CIELab values for yarn after dyeing and finishing process. The Journal of The Textile Institute. 2023; 114(9):1326-1335. doi: 10.1080/00405000.2022.2124629

[23] Chen Z, Liu J, Li J, Yuan M, Yu G. Leveraging multi-output modelling for CIELAB using colour difference formula towards sustainable textile dyeing. Autonomous Intelligent Systems. 2024; 4(1):19. doi: 10.1007/s43684-024-00076-8

[24] Wu T, Li J, Bao J, Liu Q, Jin Z, Gao J. CarbonKG: Industrial Carbon Emission Knowledge Graph-Based Modeling and Application for Carbon Traceability of Complex Manufacturing Process. Journal of Computing and Information Science in Engineering. 2024; 24(8):081001. doi: 10.1115/1.4065166